Donor–Acceptor Systems

Deutsche Ausgabe: DOI: 10.1002/ange.201500156
Internationale Ausgabe: DOI: 10.1002/anie.201500156

Charge Separation in Graphene-Decorated Multimodular Tris(pyrene)–Subphthalocyanine–Fullerene Donor–Acceptor Hybrids**

*Chandra B. KC, Gary N. Lim, and Francis D'Souza**

Abstract: *A new approach to probe the effect of graphene on photochemical charge separation in donor–acceptor conjugates is devised. For this, multimodular donor–acceptor conjugates, composed of three molecules of pyrene, a subphthalocyanine, and a fullerene C_{60} ($(Pyr)_3SubPc\text{-}C_{60}$), have been synthesized and characterized. These systems were hybridized on few-layer graphene through π–π stacking interactions of the three pyrene moieties. The hybrids were characterized using Raman, HRTEM, and spectroscopic and electrochemical techniques. The energy levels of the donor–acceptor conjugates were fine-tuned upon interaction with graphene and photoinduced charge separation in the absence and presence of graphene was studied by femtosecond transient absorption spectroscopy. Accelerated charge separation and recombination was detected in these graphene-decorated conjugates suggesting that they could be used as materials for fast-responding optoelectronic devices and in light energy harvesting applications.*

Carbon-based materials have become vital for many technological developments in the modern world. Extensive research has been performed for the last two decades on nanocarbon materials including 0D fullerenes, 1D carbon nanotubes, and 2D graphene.[1,2] Graphene, first prepared by mechanical exfoliation of graphite,[1a] is a zero bandgap semiconductor with high mobility of electrons and holes and high optical transmittance. Thus, graphene has been sought out for many scientific and technological advances including for use in building optoelectronic devices and as a transparent electrode material.[1–3]

Recently, a few studies have reported on electron-donor (or acceptor) sensitizer-functionalized graphene hybrids to probe photoinduced electron and energy transfer.[4] Both covalent and noncovalent strategies have been employed. In these hybrids, the sensitizer–graphene intra- and intermolecular interactions were expected to yield a band gap and make graphene an electron acceptor or donor, depending upon the nature of the appended sensitizer. However, evidence of charge separation in these hybrids is often challenging to establish primarily because of: a) a lack of diagnostic absorbance bands corresponding to either the reduced or oxidized forms of graphene, b) the appearance of strong optical phonon bands[5] during photoexcitation of graphene which impede spectral interpretation, and c) the close association of sensitizer to the graphene surface which makes the photophysical processes too fast to perform a systematic structure–reactivity study. These shortcomings thus warrant an altogether different approach to visualize the role of graphene on photochemical charge separation and stabilization in donor–acceptor hybrids.

In the present study, we have designed a new strategy wherein donor–acceptor conjugates, instead of a simple sensitizer, have been utilized to decorate graphene. For this, two new multimodular donor–acceptor conjugates of subphthalocyanine–fullerene tethered with three π-stacking pyrene entities (denoted $(Pyr)_3SubPc\text{-}C_{60}$; **1** and **2**), have been designed and synthesized (Figure 1). The sensitizer, subphthalocyanine (SubPc) has been chosen as an electron donor because of its nonplanar structure leaving the central boron available for further axial functionalization,[6] in this case with a familiar electron acceptor, fullerene.[7,8] Further, the macrocycle periphery is used to tether the established π-stacking pyrene moieties with spacers of variable length.[3d,9] As a result of this structural arrangement, when **1** or **2** interact with planar graphene, the C_{60} fragment (and SubPc to a lesser extent) will be away from the graphene surface (8–12 Å) giving rise to no direct interactions. To form the graphene/**1** and graphene/**2** hybrids, the donor–acceptor conjugates were treated with 2–4-layer graphene to be exfoliated and decorated with the donor-acceptor conjugates, as shown in Figure 1. To unravel the influence of π-stacking graphene on the kinetics of charge separation and charge recombination, photoinduced electron transfer in **1** and **2** and in graphene/**1** and graphene/**2** hybrids has been systematically investigated in solvents of varying polarity using femtosecond transient spectroscopy.

The synthetic details for the preparation of donor–acceptor conjugates **1** and **2** are given in the Supporting Information. Briefly, this procedure involved the preparation of tri-iodo subphthalocyanine[8e] by the reaction of 4-(4-iodophenoxy)phthalonitrile and BCl_3 in *p*-xylene. The iodo groups were replaced with either a pyrene phenoxy (for **1**) or pyrene with a long chain biphenyl (for **2**) groups. The axial chloride of SubPc was subsequently replaced with a 4-formylphenoxy group by treating the SubPc derivatives with

[*] C. B. KC, G. N. Lim, Prof. Dr. F. D'Souza
Department of Chemistry, University of North Texas
1155 Union Circle, #305070, Denton, TX 76203-5017 (USA)
E-mail: Francis.DSouza@UNT.edu

[**] We are thankful to Dr. L. D'Souza for helpful discussions. This work was supported by the National Science Foundation (Grant No. 140188 to F.D.).

Supporting information for this article (including structures of $(Pyr)_3SubPc$ and SubPc control compounds, UV/Vis absorption, emission, and femtosecond transient absorption spectra, and DPV plots of **1** and graphene/**1** hybrids, synthetic details and characterization of **1** and **2**, and the experimental section) is available on the WWW under http://dx.doi.org/10.1002/anie.201500156.

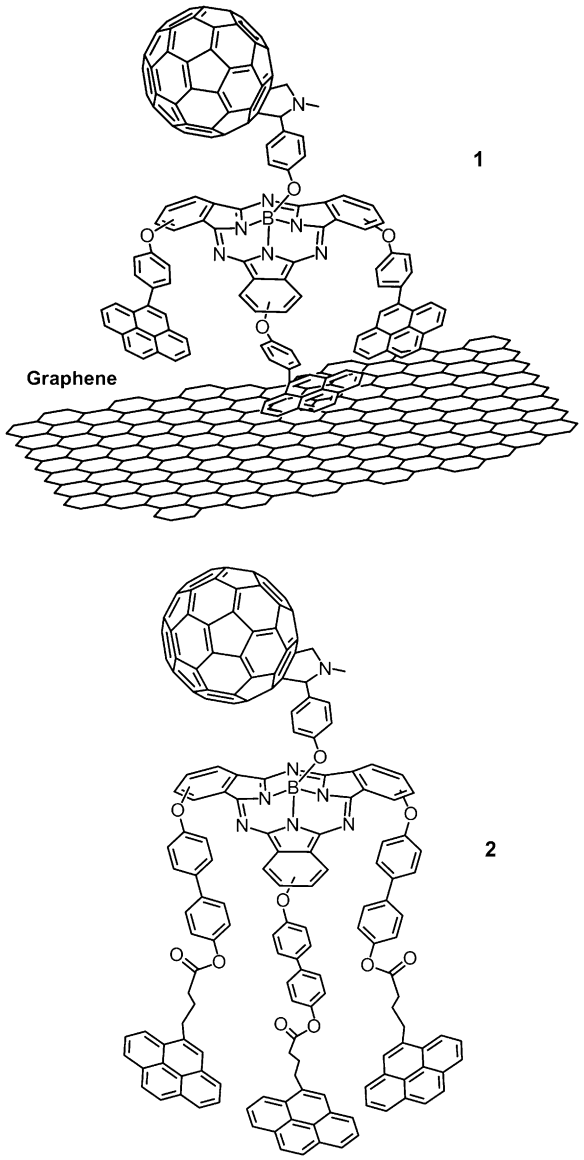

Figure 1. Structure of the subphthalocyanine–fullerene donor–acceptor conjugates **1** and **2** tethered with three pyrene units. As shown for **1**, these conjugates interact with graphene through π–π stacking between the pyrene units and graphene to form graphene/**1** and graphene/**2** hybrids.

4-hydroxybenzaldehyde in toluene. Finally, the SubPc derivatives were treated with C_{60} and sarcosine in toluene[10] followed by chromatographic purification to obtain **1** and **2**. The newly synthesized conjugate was fully characterized by NMR (^{1}H and ^{13}C), MALDI-TOF mass spectrometry, and spectroscopic and electrochemical methods.

Figure 2a shows the UV/Vis absorption spectrum of **2** and the control compounds pyrene, *t*BuSubPc, and $(Pyr)_3$SubPc (**2a**) in benzonitrile. The relevant absorption spectra for **1** and its precursors are given in Figure S1 in the Supporting Information. The UV/Vis absorption spectrum of compound **2** showed absorption bands at $\lambda = 315$, 330, 346, 432, and 574 nm. The first three bands corresponded that of pyrene, the peak at $\lambda = 432$ nm was attributed to fulleropyrrolidine, and the $\lambda = 574$ nm band corresponded to SubPc. Appending a C_{60} moiety had no effect on the absorption band of the conjugate at 574 nm while this band was about 8 nm red-shifted compared with pristine SubPc without pyrene tethers. The tethered pyrene peaks were also red-shifted by 7 nm compared to pristine pyrene, primarily as a result of covalent functionalization. Similar results were obtained for **1** (see Figure S1a), however, the pyrene absorption bands in the $\lambda =$ 315–360 nm region were broad and appeared as shoulder bands to the main band at 347 nm. These results suggest the occurrence of some intramolecular interactions between the pyrene and the SubPc units within the conjugate. As shown in Figure 2b and Figure S1b, in the fluorescence spectra of the precursor $(Pyr)_3$SubPc derivatives (**2a** and **1a**; see Scheme S1 for the structures) emission bands appeared at $\lambda = 594$ nm and were red-shifted by nearly 12 nm compared to pristine SubPc. In **1** and **2**, the SubPc emission was found to be quantitatively quenched (over 97% of its original intensity) suggesting occurrence of excited-state events from the ^{1}SubPc* state (Figure 2b and Figure S1b).

As shown in Figure S2, the spectral trends in toluene were quite similar to those discussed in benzonitrile. Additionally, the fluorescence quenching of SubPc in **1** and **2** in nonpolar toluene was also very high (over 95%).

To prepare the graphene/**1** and graphene/**2** hybrids, first, 2–4-layer graphene was dispersed in benzonitrile or toluene (2 mg in 20 mL) for exfoliation by sonication and centrifugation. Aliquots of the clear brown solution of graphene obtained after filtration was added to a solution of **1** or **2** in the solvent of choice. Spectral changes associated with this addition in benzonitrile are shown in Figure 2c and Figure S1c. Similar trends were also detected in toluene. The changes included diminished intensity of the band at $\lambda =$ 575 nm and an increase in absorbance in the 330–500 nm range as a result of interactions with graphene. An isosbestic point at $\lambda = 594$ nm for **1** and **2** was also detected indicating the existence of an equilibrium process for the interaction between the conjugate and graphene.

To establish the energy levels relevant to probe the excited-state events of the conjugate in the absence and presence of graphene, electrochemical studies were performed using the differential pulse voltammetry (DPV) technique. Figure 2d and Figure S1d, respectively, show DPVs of **2** and **1** (black lines) in benzonitrile containing 0.1 M $(TBA)ClO_4$. On the basis of these voltammograms and from additional experiments involving control compounds, the site of electron transfer could be deduced. The first anodic process of **2** and **1** occurred at $+0.53$ V versus Fc/Fc^+ (ferrocene/ferrocenium) corresponding to the oxidation of the SubPc entity. Cyclic voltammetry studies confirmed these processes to be reversible. The second oxidation process, corresponding to the oxidation of pyrene subunits, appeared at $+0.76$ V for **1** and $+0.70$ V for **2**. Considering cathodic processes, the first reversible reduction, corresponding to C_{60}, was located at -1.02 V whereas the second reduction for both **1** and **2** around -1.44 V could be attributed to two overlapped processes, specifically the second reduction of C_{60} and first reduction of the SubPc unit. At more negative and positive potentials, additional irreversible redox processes were also

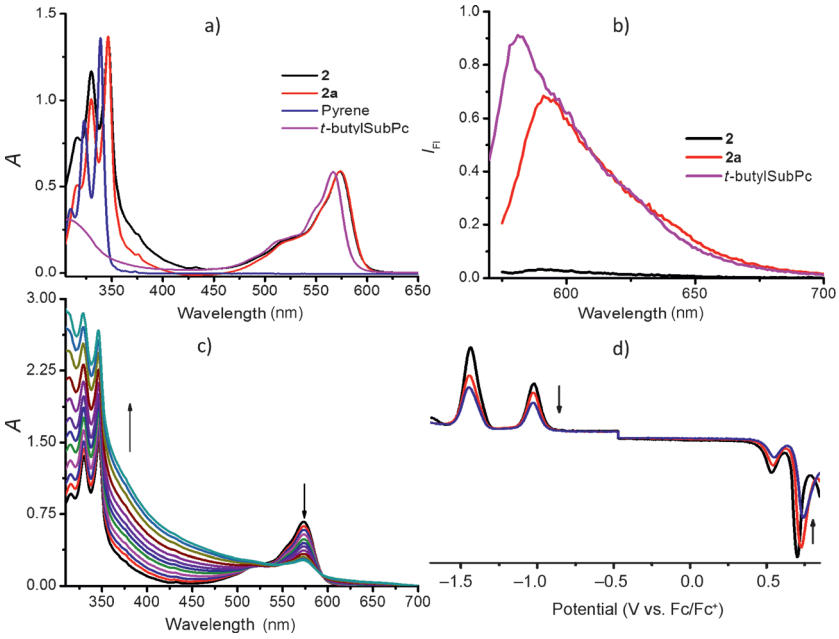

Figure 2. a) UV/Vis absorption and b) fluorescence spectra ($\lambda_{ex}=574$ nm) of compounds **2**, **2a**, pyrene, and *t*BuSubPc in benzonitrile. c) UV/Vis absorption spectral changes upon addition of aliquots of 2–4-layer graphene to a solution **2** in benzonitrile showing the interaction of graphene with **2**. d) Differential pulse voltammograms of **2** (black line) upon increasing addition of graphene in benzonitrile containing 0.1 M (TBA)ClO_4. TBA = tetrabutylammonium.

detected. Addition of graphene to the electrolyte solution diminished the current (slower diffusion because of increased mass of the hybrids) with noticeable changes in the redox potential of SubPc and pyrene but not that of C_{60}. That is, the SubPc oxidation became more difficult by about 25 mV whereas that for pyrene oxidation became approximately 35 mV more difficult for both graphene/**1** and graphene/**2** hybrids. These observations are in good agreement with our earlier hypothesis that the structure of **1** and **2** allow pyrene and, to a lesser extent, SubPc interactions with graphene, leaving C_{60} unperturbed. Using the redox and spectroscopic data, free-energy calculations (ΔG_{CS}) for the occurrence of photoinduced electron transfer originating from the ^{1}SubPc* ($E_{0\text{-}0}=2.12$ eV) and $^1C_{60}$* ($E_{0\text{-}0}=1.75$ eV) excited states were performed using the Rehm–Weller approach[11,12] (neglecting the solvation term). Such calculations revealed that the formation of the $(Pyr)_3SubPc^{\bullet+}$–$C_{60}^{\bullet-}$ charge-separated states from both ^{1}SubPc* and $^1C_{60}$* are exothermic processes. ΔG_{CS} values from ^{1}SubPc* in benzonitrile were −0.57 eV for both **1** and **2**, and −0.54 eV for graphene/**1** and graphene/**2** hybrids. In the same way, ΔG_{CS} values of −0.20 eV for both **1** and **2**, and −0.18 eV for graphene/**1** and graphene/**2** hybrids were obtained from $^1C_{60}$* in benzonitrile. In toluene, the energy level of the radical ion pairs would be exothermic by another 150–200 mV than that computed in benzonitrile.

Raman spectra of the graphene/**1** and graphene/**2** hybrids along with that of pristine 2–4-layer graphene is shown in Figure 3a. Briefly, in agreement with previous reports,[13] a G band for graphene was detected at 1580 cm^{-1} with a much weaker D band appearing at 1350 cm^{-1} and a D′ band appeared as a shoulder to the G band at 1610 cm^{-1}. The intensity ratio for the G:D bands was around 5.0. Interestingly, for graphene/**1** and graphene/**2** hybrids, the G band appeared at 1610 cm^{-1} and the D band at 1345 cm^{-1} with an intensity ratio of nearly 1.0. The Raman spectral features were close to that reported for graphene oxide,[14] suggesting effective functionalization of graphene with the current noncovalent approach. The HRTEM image of graphene/**1** in Figure 3b shows exfoliated graphene, although few-layer graphene are detected as a result of aggregation during sample preparation. Thus, in the studied hybrids, the graphene could be considered to be essentially a monolayer to a few layers.

Next, photochemical processes in **1** and **2** conjugates and graphene/**1** and graphene/**2** hybrids were investigated by femtosecond transient spectroscopy in both polar benzonitrile and nonpolar toluene solutions. Formation of $SubPc^{\bullet+}$ is expected to result in the appearance of a band at $\lambda=685$ nm while for $C_{60}^{\bullet-}$ a band at $\lambda=1020$ nm is expected during electron transfer.[8] As shown in Figure 4 and Figure S3, upon

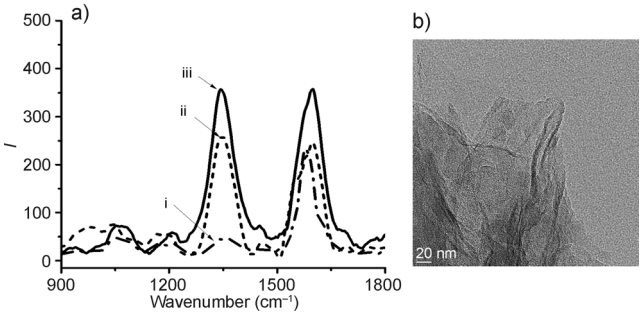

Figure 3. a) Raman spectra of few-layer graphene (i), and graphene/**1** (ii) and graphene/**2** (iii) hybrids. b) HRTEM image of the graphene/**1** hybrid. Scale bar = 20 nm.

excitation of **1** and **2** at $\lambda=400$ nm, an instantaneous formation of ^{1}SubPc* (depleted band in the 570 nm range)[8] and $^1C_{60}$* (absorbance in the 900–950 nm range)[15] were detected. The formation of $^1C_{60}$* could be due to direct excitation of C_{60} or the product of ultrafast energy transfer from ^{1}SubPc*.

The formation of $(Pyr)_3SubPc^{\bullet+}$–$C_{60}^{\bullet-}$ charge separated state from the initial ^{1}SubPc* or $^1C_{60}$* in **1** and **2** was confirmed from the $C_{60}^{\bullet-}$ band at $\lambda=1020$ nm and the $SubPc^{\bullet+}$ band in the range 650–700 nm. The radical ion-pair bands, after reaching a maximum, started decaying because of the charge recombination process. The rates of charge separation k_{CS} and charge recombination k_{CR} were evaluated by monitoring the rise and decay time profile of the $C_{60}^{\bullet-}$ band at 1020 nm (as shown in Figure 4). Notably, as predicted for

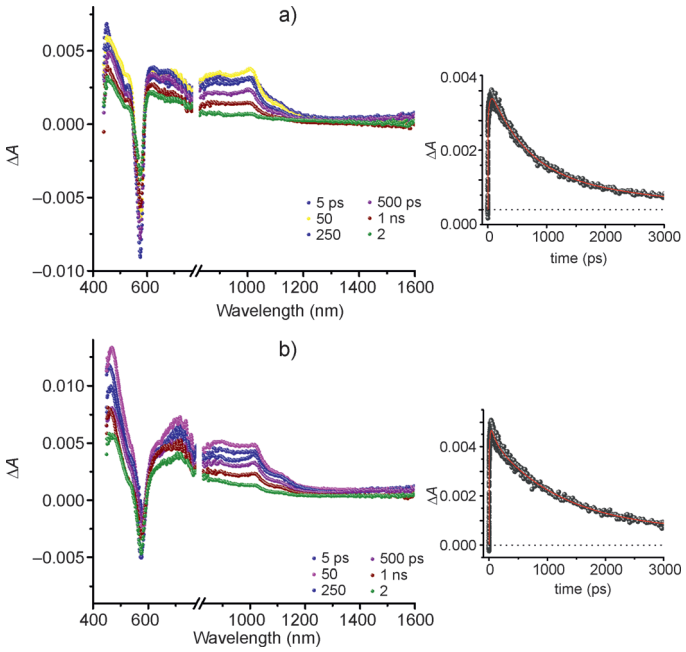

Figure 4. Femtosecond transient absorption spectra of **2** in Ar-saturated a) benzonitrile and b) toluene at the indicated time intervals. Time profiles of the $\lambda = 1020$ nm band corresponding to the fullerene anion radical are shown in the plots on the right-hand side.

fullerenes, the recombination process was much slower than the charge separation process with considerable radical peak intensities lasting over 3 ns, the time window of the instrument. In such a case, the determined k_{CR} values could be considered as the lower limit. The kinetic values are given in Table 1 which reveal fast charge separation and relatively slow charge recombination and the expected solvent effect on electron-transfer kinetics.[16] That is, facile charge separation and recombination in polar benzonitrile over nonpolar toluene was evident.

Table 1: Rates of charge separation (k_{CS}) and charge recombination (k_{CR}) obtained for conjugates **1** and **2** and their graphene hybrids.

System	Solvent	k_{CS} [s^{-1}]	k_{CR} [s^{-1}]
1	benzonitrile	2.6×10^{10}	9.8×10^{8}
	toluene	2.3×10^{10}	6.8×10^{8}
2	benzonitrile	2.5×10^{10}	9.1×10^{8}
	toluene	1.7×10^{10}	6.9×10^{8}
Graphene/**1**	benzonitrile	6.9×10^{11}	1.5×10^{9}
	toluene	1.5×10^{11}	3.0×10^{9}
Graphene/**2**	benzonitrile	6.8×10^{11}	1.3×10^{9}
	toluene	3.4×10^{11}	2.7×10^{9}

Having established charge separation in these conjugates, we focused our attention on the graphene/**1** and graphene/**2** hybrids. Figure 5 and Figure S4 show the femtosecond transient absorption spectra of the hybrids in benzonitrile and toluene, respectively. Immediately after excitation (see the spectrum at 1 ps), transient features corresponding to ^{1}SubPc* and $^1C_{60}$*, and strong optical phonon peaks of graphene appeared as negative peaks in the $\lambda = 690$ nm and 1200 nm ranges (see Figure S5 for femtosecond transient spectra of pristine few-layer graphene and peak time profiles in both benzonitrile and toluene). Recovery of these signals was fast, that is, in less than 5 ps much of the intensity was recovered, similar to that of pristine few-layer graphene (Figure S5). The excited state decay resulted in the concomitant formation of radical ion-pair peaks corresponding to the formation of a graphene/$(Pyr)_3SubPc^{\bullet+}$–$C_{60}^{\bullet-}$ radical ion pair in these hybrids, revealing successful charge separation in the hybrids.

The k_{CS} and k_{CR} values for the graphene/**1** and graphene/**2** hybrids were evaluated using a procedure similar to that used for the conjugates, **1** and **2**, that is, by monitoring the growth and decay of $C_{60}^{\bullet-}$. These time profiles are shown in the right-hand side panels in Figure 5 and Figure S4, and reveal faster charge separation and charge recombination than that observed for **1** and **2** lacking graphene. Accordingly, the estimated k_{CS} and k_{CR} values of graphene/**1** and graphene/**2** hybrids were found to be nearly an order of magnitude higher compared to that of conjugates **1** and **2**. These results show accelerated charge separation and subsequent charge recombination in the graphene/**1** and graphene/**2** hybrids. It should also be mentioned here that the k_{CS} parameter is only an estimated value as contributions for optical phonon bands of graphene at early timescales masked the $C_{60}^{\bullet-}$ growth signal to some extent.

The observed charge separation and charge recombination in the graphene hybrids merit some discussions. For both $(Pyr)_3SubPc$–C_{60} conjugates, the similar magnitude of the k_{CS} values in polar and nonpolar solvents suggests that the forward electron-transfer process belongs to the top section of the Marcus parabola[17] where the solvent effects on electron-transfer kinetics are minimal. The k_{CS} values of graphene/

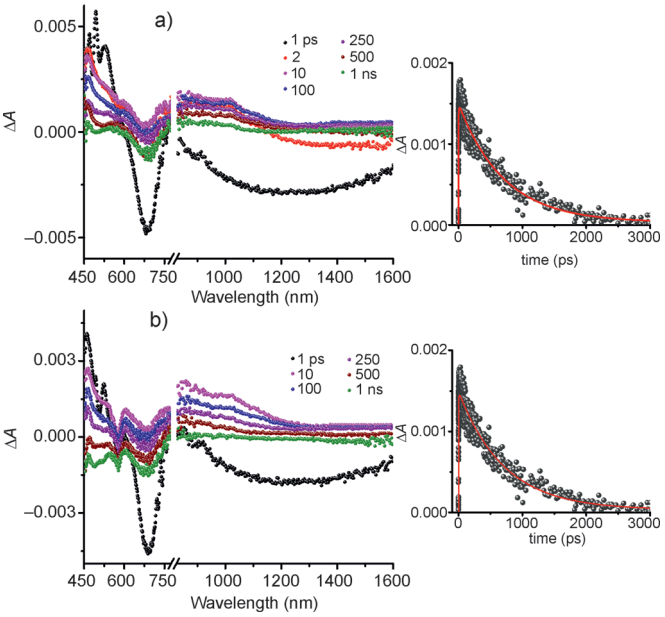

Figure 5. Femtosecond transient absorption spectra of the graphene/**2** hybrid in Ar-saturated a) benzonitrile and b) toluene at the indicated time intervals. Time profiles of the $\lambda = 1020$ nm band corresponding to the decay of the fullerene anion radical are shown in the plots on the right-hand side.

$(Pyr)_3SubPc–C_{60}$ hybrids also suggest such a trend. The small decrease in ΔG_{CS} values for the hybrids as compared to those of the conjugates as a result of redox modulation predicts slightly higher k_{CR} values. In addition to the energetics, the geometry of the graphene/$(Pyr)_3SubPc–C_{60}$ hybrids or any defects in the graphene might also contribute to this behavior.

In summary, we have synthesized novel multimodular, $(Pyr)_3SubPc–C_{60}$ conjugates and demonstrated the occurrence of photoinduced electron transfer leading to charge separation. Next, the donor–acceptor conjugates were stacked on graphene using the pyrene tethers on the SubPc macrocycle through π–π stacking interactions, leaving the axial fullerene unit far from the graphene surface. The graphene/$(Pyr)_3SubPc–C_{60}$ hybrids were characterized by UV/Vis absorption, electrochemical, Raman, and HRTEM methods. The measured redox potentials revealed redox modulation of the pyrene and SubPc units leaving C_{60} unperturbed because of its distant position from the graphene surface, as anticipated by our supramolecular design strategy. Femtosecond transient absorption studies showed the occurrence of electron transfer leading to the formation of a graphene/$(Pyr)_3SubPc^{\bullet+}–C_{60}^{\bullet-}$ charge separated state in the hybrids. In other words, the presence of graphene in the hybrid did not obstruct the donor and acceptor properties of the conjugate. Interestingly, the estimated k_{CS} and k_{CR} values were nearly an order of magnitude higher in the case of the hybrids compared to those values obtained for the corresponding conjugates, showing accelerated photochemical/photophysical processes caused by the presence of graphene. These results highlight the potential importance of the graphene/$(Pyr)_3SubPc–C_{60}$ hybrids which may be useful as materials in building fast-responding optoelectronic devices (picosecond timescale) and in light-to-electricity and light-to-fuel conversion applications. Currently we are looking into these possibilities using hybrids built on this strategy.

Keywords: charge separation · donor–acceptor systems · fullerenes · graphene · subphthalocyanines

How to cite: *Angew. Chem. Int. Ed.* **2015**, *54*, 5088–5092
Angew. Chem. **2015**, *127*, 5177–5181

[1] a) A. K. Geim, K. S. Novoselov, *Nat. Mater.* **2007**, *6*, 183–191; b) A. K. Geim, *Science* **2009**, *324*, 1530–1534; c) C. N. R. Rao, A. K. Sood, K. S. Subrahmanyam, A. Govindaraj, *Angew. Chem. Int. Ed.* **2009**, *48*, 7752–7777; *Angew. Chem.* **2009**, *121*, 7890–7916; d) M. J. Allen, V. C. Tung, R. B. Kaner, *Chem. Rev.* **2010**, *110*, 132–145; e) Z. Sun, D. K. James, J. M. Tour, *J. Phys. Chem. Lett.* **2011**, *2*, 2425–2432.

[2] a) *Handbook of Carbon Nanomaterials*, *Vols. 1–6* (Eds.: F. D'Souza, K. M. Kadish), World Scientific Publications, Singapore, **2011**, **2012**, **2014**; b) *Organic Nanomaterials* (Eds.: T. Torres, G. Bottari), Wiley, Hoboken, NJ, **2013**.

[3] a) S. Watcharotone, D. A. Dikin, S. Stankovich, R. Piner, I. Jung, G. H. B. Dommett, G. Evmenenko, S. E. Wu, S. F. Chen, C. P. Liu, S. T. Nguyen, R. S. Ruoff, *Nano Lett.* **2007**, *7*, 1888–1892; b) P. Blake, P. D. Brimicombe, R. R. Nair, T. J. Booth, D. Jiang, F. Schedin, L. A. Ponomarenko, S. V. Morozov, H. F. Gleeson, E. W. Hill, A. K. Geim, K. S. Novoselov, *Nano Lett.* **2008**, *8*, 1704–1708; c) X. Wang, L. Zhi, K. Müllen, *Nano Lett.* **2008**, *8*, 323–327; d) K. S. Kim, Y. Zhao, H. Jang, S. Y. Lee, J. M. Kim, K. S. Kim, J. H. Ahn, P. Kim, J. Y. Choi, B. H. Hong, *Nature* **2009**, *457*, 706–710.

[4] a) J. Malig, N. Jux, D. Kiessling, J. J. Cid, P. Vazquez, T. Torres, D. M. Guldi, *Angew. Chem. Int. Ed.* **2011**, *50*, 3561–3565; *Angew. Chem.* **2011**, *123*, 3623–3627; b) J. Malig, C. Romero-Nieto, N. Jux, D. M. Guldi, *Adv. Mater.* **2012**, *24*, 800–805; c) F. Li, H. Yang, C. Shan, Q. Zhang, D. Han, A. Ivaska, L. J. Niu, *Mater. Chem.* **2009**, *19*, 4022–4025; d) C. B. KC, S. K. Das, K. Ohkubo, S. Fukuzumi, F. D'Souza, *Chem. Commun.* **2012**, *48*, 11859–11861; e) S. M. Aly, M. R. Parida, E. Alarousu, O. F. Momammed, *Chem. Commun.* **2014**, *50*, 10452–10455.

[5] a) L. Huang, G. V. Hartland, L.-Q. Chu, Luxmi, R. M. Feenstra, C. Lian, K. Tahy, H. Xing, *Nano Lett.* **2010**, *10*, 1308–1313; b) J. Shang, T. Yu, G. G. Gurzadyan, *Appl. Phys. B* **2012**, *107*, 131–136; c) F. Carbone, G. Aubock, A. Cannizzo, F. V. Mourik, R. R. Nair, A. K. Geim, K. S. Novoselov, M. Chergui, *Chem. Phys. Lett.* **2011**, *504*, 37–40.

[6] a) C. G. Claessens, D. Gonzalez-Rodrıguez, T. Torres, *Chem. Rev.* **2002**, *102*, 835–854; b) N. Kobayashi, *Coord. Chem. Rev.* **2002**, *227*, 129–152; c) C. G. Claessens, D. Gonzalez-Rodriguez, M. S. Rodriguez-Morgade, A. Medina, T. Torres, *Chem. Rev.* **2014**, *114*, 2192–2277.

[7] a) Q. Xie, E. Perez-Cordero, L. Echegoyen, *J. Am. Chem. Soc.* **1992**, *114*, 3978–3980; b) H. Imahori, K. Tamaki, D. M. Guldi, C. Luo, M. Fujitsuka, O. Ito, Y. Sakata, S. Fukuzumi, *J. Am. Chem. Soc.* **2001**, *123*, 2607–2617.

[8] For examples of subphthalocyanine–fullerene donor–acceptor conjugates, see: a) D. González-Rodríguez, T. Torres, D. M. Guldi, J. Rivera, L. Echegoyen, *Org. Lett.* **2002**, *4*, 335–338; b) D. González-Rodríguez, T. Torres, D. M. Guldi, J. Rivera, M. A. Herranz, L. Echegoyen, *J. Am. Chem. Soc.* **2004**, *126*, 6301–6313; c) D. González-Rodríguez, T. Torres, M. A. Herranz, L. Echegoyen, E. Carbonell, D. M. Guldi, *Chem. Eur. J.* **2008**, *14*, 7670–7679; d) D. González-Rodríguez, E. Carbonell, D. M. Guldi, T. Torres, *Angew. Chem. Int. Ed.* **2009**, *48*, 8032–8036; *Angew. Chem.* **2009**, *121*, 8176–8180; e) C. B. KC, G. N. Lim, F. D'Souza, *Org. Lett.* **2013**, *15*, 4612–4615.

[9] J. A. Mann, J. Rodriquez-Lopez, H. D. Abruna, W. R. Dichtel, *J. Am. Chem. Soc.* **2011**, *133*, 17614–17617.

[10] M. Maggini, G. Scorrano, M. Prato, *J. Am. Chem. Soc.* **1993**, *115*, 9798–9799.

[11] D. Rehm, A. Weller, *Isr. J. Chem.* **1970**, *8*, 259–271.

[12] $\Delta G^S_{CS} = \Delta E_{0\text{-}0} - e(E_{ox} - E_{red})$, $\Delta E_{0\text{-}0}$ is the energy of the lowest excited state ($^1SubPc^* = 2.12$ eV and $^1C_{60}^* = 1.75$ eV). The symbols E_{ox} and E_{red} represent the first oxidation potential of the electron donor SubPc and the first reduction of the electron acceptor fullerene, respectively.

[13] C. Ferrari, *Solid State Commun.* **2007**, *143*, 47–57.

[14] V. C. Tung, M. J. Allen, Y. Yang, R. B. Kaner, *Nat. Nanotechnol.* **2009**, *4*, 25–29.

[15] S. K. Das, A. Mahler, A. K. Wilson, F. D'Souza, *ChemPhysChem* **2014**, *15*, 2462–2472.

[16] a) H. Imahori, K. Hagiwara, M. Aoki, T. Akiyama, S. Taniguchi, T. Okada, M. Shirakawa, Y. Sakata, *J. Am. Chem. Soc.* **1996**, *118*, 11771–11782; b) C. B. KC, G. N. Lim, V. N. Nesterov, P. A. Karr, F. D'Souza, *Chem. Eur. J.* **2014**, *20*, 17100–17112.

[17] R. A. Marcus, *Angew. Chem. Int. Ed. Engl.* **1993**, *32*, 1111–1121; *Angew. Chem.* **1993**, *105*, 1161–1172.

Received: January 7, 2015
Revised: February 11, 2015
Published online: February 27, 2015

